Article

Development of in-line measurement techniques for monitoring powder characteristics in a multi-stage spray drying process

Jennifer Frank[1,*,†], Tobias V. Raiber[1,*,†], Laura Grotenhoff[1] and Reinhard Kohlus[1]

[1] Department of Process Engineering and Food Powders, University of Hohenheim, Garbenstraße 25, 70599 Stuttgart, Germany
* Correspondence: jennifer.frank@uni-hohenheim.de (J.F.), tobias.raiber@uni-hohenheim.de (T.R.)
† These authors contributed equally to this work.

Abstract: The integration of spray drying and agglomeration offers significant advantages, such us continuous production with lower energy consumption. However, it is a knife-edge process with a narrow operating window and limited degrees of freedom that decide between successful agglomeration and fluidized bed blockage due to excessive moisture. In this contribution, factors influencing the spray-through agglomeration process of skim milk powder as a model system were investigated via a design of experiments. Three in-line monitoring methods were applied and tested to observe the most important parameters in the agglomeration process: product moisture and particle size distribution. Regarding the moisture content, a capacitive moisture sensor was calibrated with linear regression and a near-infrared sensor with partial least squares regression. Near-infrared spectroscopy was found to be the suitable method for determining moisture content, while the capacitive moisture sensor mainly provides information on the bulk density, the filling level or fluidization state in the fluidized bed. Additionally, particle size distribution data was extracted from the spectral data using in-line data of a spatial filter velocimetry probe in the fluidized bed. This opens the potential to monitor both parameters in real-time with a single non-invasive sensor.

Keywords: Process integration, In-line measurement, Capacitive moisture measurement, Near-infrared spectroscopy, Fluidized bed agglomeration, Spray drying

1. Introduction

Skim milk powder (SMP) is a frequently used ingredient in various food applications including infant formula, ice cream, confectionery and bakery [1, 2]. The powder is typically produced by spray drying, where liquid skim milk concentrate is atomized into fine drops and then dried in a stream of hot air, resulting in a bulk solid. The size of the drops, as well as the inlet and outlet air temperatures, can be adjusted to control the final particle size of the SMP. However, a major challenge with this process is the generation of fine material [2, 3]. These fine particles cause problems in certain applications due to their dusting properties and poor wettability. This makes it challenging for customers to effectively incorporate the product into their formulations, as they may struggle to achieve a consistent mix and accurate dosing [4, 5].

To improve the product quality SMP can be further processed by agglomeration to increase its flowability, solubility, and dispersibility [3, 5]. An effective agglomeration equipment is a fluidized bed [6 – 8], where a bulk solid is subjected to a flow of heated gas, which causes the particles to behave in a fluid-like manner. A binding agent or plasticizer, such as water, is then sprayed onto the particles. Collisions of moist surfaces cause them to form clusters through the formation of liquid bridges, which are solidified by the evaporation of the solvent [8].

Besides batch processes, integrated spray drying and agglomeration solutions have been reported in literature as design concepts since the 1980s. Their development was driven by the need for more efficient and cost-effective powder manufacturing processes,

 doi:10.20944/preprints202306.0844.v1

especially for more difficult-to-dry products such as fine or sticky materials [9]. These integrated solutions have the advantage of being able to perform the entire production process in a single plant and also allow for continuous production. They also have certain disadvantages, such as increased process complexity. The mean residence time, i.e. the agglomeration time, is determined by the installed bed volume and the throughput of the spray dryer. Spraying too much binder in this time interval will result in sticky material and bed blockage, spraying too little will not achieve the target particle size and therefore the target powder properties making this a knife-edge process. One of the most important parameters for forced agglomeration with binding agents is the product moisture content. Monitoring the moisture content is thus crucial, as it directly impacts the formation and properties of the agglomerates. In addition, it ensures effective use of binding agent and energy. Properly implemented, operating parameters, such as the fluidization air velocity or binding agent amount, can be adjusted as needed to achieve the required particle size and shape [8, 10].

Measurement technology can be used to monitor and control these parameters. By utilizing reliable and widespread methods, like temperature and mass flow rate measurements, only process conditions can be monitored. Advanced techniques are needed to measure product moisture and particle size, but sampling-based methods are not suitable for real-time control. Methods like near-infrared spectroscopy (NIR) and dielectric properties (CM: capacitance measurement) for moisture, as well as spatial filter velocimetry (IPP: in-line particle probe), focused beam reflectance measurement (FBRM) or even image analysis for particle size, can be used [11 – 13]. In some cases, attempts have been made to determine basic size information in addition to moisture from NIR spectral data [14]. Multi-sensor approaches are already available, but mostly in the context of individual unit operations and not in the integrated spray agglomeration process [13]. Advanced monitoring and control strategies are especially needed for a continuous integrated process as bed blockages lead to a shutdown of the entire process. However, the implementation is more challenging due to the high complexity.

The practical implementation for this study involved a pilot-scale two-stage spray-through agglomeration process with an integrated fluidized bed. Fluidization velocity, temperature, and the amount of moisture injected into the system were varied within the scope of a full factorial design of experiments. In addition, further trials were conducted to optimize the agglomeration process and expand the data set. The integrated fluidized bed was equipped with measurement ports allowing for the simultaneous operation of two sensors, NIR, CM or IPP. The sensors used in this study vary in terms of measurement location as well as principle, they can be non-invasive (NIR) or invasive (CM, IPP) and thus come into contact with the product. The former can be operated through a glass window. From a hygienic perspective, non-invasive techniques are preferred in the context of food production.

The objective of this work was to optimize the two-stage spray-through agglomeration process with an integrated fluidized bed. An in-line-monitoring system was established with special focus on the product moisture content and the particle size. The use of these measurement techniques allows the monitoring and controlling of the agglomeration process. This is particularly important with respect to the moisture added to the system with a binder, regardless of varying air temperature and mass flow, enabling to achieve the desired powder properties within the short residence time of a two-stage spray dryer without risking a bed blockage.

2. Materials and Methods

The study involved calibration and validation trials using skim milk that had been dried using a spray-through method in a pilot-scale spray dryer. A detailed explanation of the spray drying process is given below.

2.1 Spray drying and agglomeration

Preprints (www.preprints.org) | NOT PEER-REVIEWED | Posted: 12 June 2023 doi:10.20944/preprints202306.0844.v1

The starting material was low heat SMP (Sachsenmilch Leppersdorf GmbH, Leppersdorf, Germany) which was rehydrated with demineralized water to a total solid content of 30 %. The concentrate was then atomized using either a Schlick type 100 hollow cone pressure nozzle (Düsen-Schlick Coburg, Germany) with orifice diameters between 0.3 and 0.5 mm and a pressure of 8 MPa, or a two-fluid nozzle (GEA Niro Søborg, Denmark) with an orifice of 2 mm. The two-fluid nozzle was operated at a constant air-to-liquid ratio (ALR = 1) to ensure comparable droplet sizes at varying mass flow rates [15]. The mass flow rate was adjusted to maintain a constant outlet temperature of 75 °C at varying process conditions.

The multi-stage drying process, including the fines return and nozzle zone agglomeration, is described in detail in [16]. Beyond that, the process parameters were optimized for the product with the inlet air temperature set to 200 °C, drying air mass flow to 200 kg h^{-1} and the fines return airflow to 25 kg h^{-1}. On average, the selected spray conditions correspond to a solids mass flow of about 60 g min^{-1}. The perforated plate in the fluidized bed had a pressure drop of 510 Pa at an empty pipe fluidization air velocity of 0.8 m s^{-1}.

A second two-fluid nozzle Schlick type 970/7-1 S 1 (Düsen-Schlick Coburg, Germany) with an orifice diameter of 0.8 mm was mounted into the fluidized bed as a bottom-spray configuration. Water was introduced into the fluidized bed at rates between 0 and 18 g min^{-1} as binding agent. The cap was set on position four. To measure the properties of the agglomerates formed, measurement ports were mounted at a distance of 60 and 160 mm above the perforated plate.

The equipment configuration is shown in Figure 1. The fluidized bed is located below the spray dryer with the fluidization air entering through a perforated plate and exiting the system at the top of the spray dryer. Either the IPP or CM sensor is mounted on measurement port one. While the IPP sensor protrudes into the fluidized bed, the NIR sensor is mounted on sapphire glass at port two. Powder discharge is automated to maintain a constant residence time and filling level based on differential pressure (sensor 3). The discharge valve triggered for 0.2 seconds as soon as the bulk material causes a pressure drop of 140 Pa.

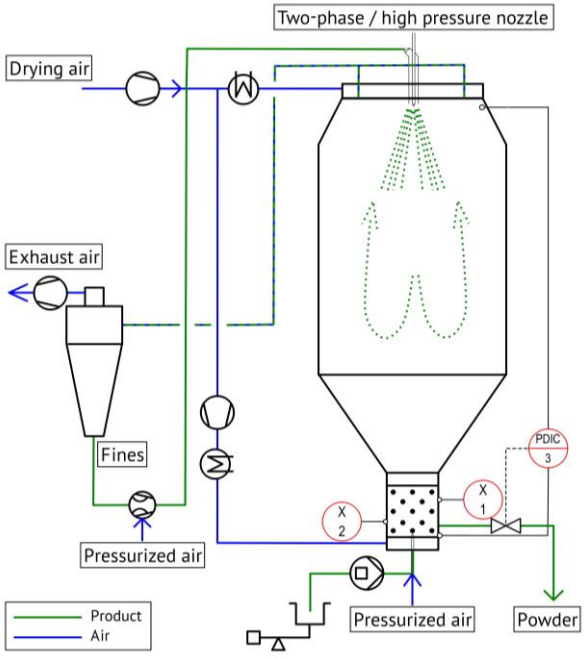

Figure 1. Spray through agglomeration system with an integrated NIR, CM or IPP sensor.

Different combinations of measurement probes were used to gather the necessary data. These combinations included the NIR and IPP probe, the NIR probe and CM sensor, or the CM sensor at the lower position and the IPP at the upper position. This approach

Preprints (www.preprints.org) | NOT PEER-REVIEWED | Posted: 12 June 2023 doi:10.20944/preprints202306.0844.v1

allowed the simultaneous measurement of different properties using different probes. However, it should be noted that the measuring positions did not always align in every comparison.

2.2 Experimental design

A total of N = 85 individual trials were conducted for calibration and validation. 18 of these trials were part of a full factorial design of experiments (DoE) with three parameters, two levels, and the inclusion of the center point. The DoE was duplicated into two blocks with one block for each nozzle type. The remaining trials were performed as preliminary tests for optimization and additional systematic trials for calibration (blue circles in Figure 2). 26 of the 85 trials were conducted using the high-pressure nozzle. The data were randomly split into a calibration and validation set in a 7:3 ratio, with 60 data sets being used for the calibration of the model.

An excerpt from the experimental design is shown in Figure 2. The binder addition rate was varied equidistantly from 0 to 5 g min^{-1}, the temperature was also varied equidistantly from 60 to 100 °C and the fluidization velocity from 0.6 to 1 m s^{-1}.

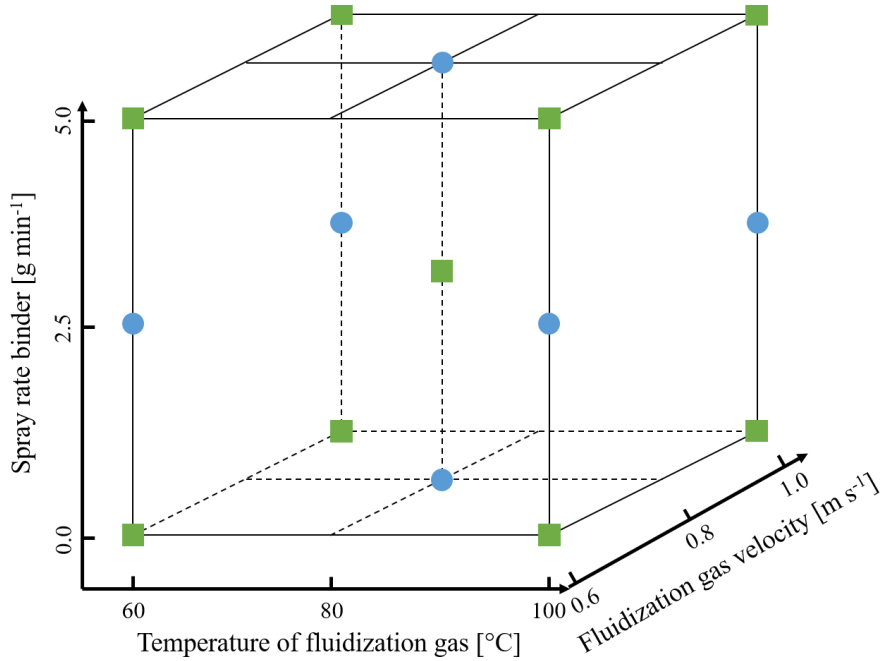

Figure 2. Excerpt from the experimental design used in this study. Green squares: full factorial DoE. Blue circles: systematic extension for calibration.

2.3 Capacitive moisture measurement

The Litronic FMS II (Liebherr-Mischtechnik GmbH, Bad Schussenried, Germany) was used for capacitive moisture measurement by measuring the dielectric properties of the agglomerates. With changing moisture content, the dielectric properties of the matrix changes, which is represented at the output as a change in voltage. [17] The sensor had a sampling cycle of one measurement per second and was positioned flush with the wall. The corresponding values from the capacitive sensor were collected over 30 seconds for each measurement and then averaged to obtain an accurate representation of the dielectric properties.

2.4 Near-infrared spectroscopy

NIR spectra were recorded via reflection using a Polytec contact probe PSS-H-B02 version 1.7 (Polytec GmbH, Waldbronn, Germany) equipped with a fiber optic system and a halogen lamp. The probe was connected to a PSS 1720 spectrometer over a 3 m optical fiber cable. The software PAS-LAB version 1.2 was used for settings and exporting

 doi:10.20944/preprints202306.0844.v1

the NIR spectra taken. The spectra were obtained with an exposure time of 7 ms and 500 accumulators covering a wavelength range from 850 to 1650 nm with 401 measurement points. Dark and reference measurements were performed prior to each measurement. Offline spectra were taken in triplicate (100 accumulation) with a measurement cylinder, which was filled approximately to a height of 150 mm.

Partial least squares (PLS) regression was used for calibration. The samples were randomly split 70:30 in a calibration and validation data set. An in-house developed Matlab® (MathWorks, Natick, USA) program automatically tested different number of factors, preprocessings and responses based on statistical parameters. The statistical parameters are: coefficient of determination (R^2), root mean square error (RMSE), standard error (SE), as well as systematic error (Bias). Wavelength and sample selections were tested, but will not be shown in this work.

2.5 Spatial filter velocimetry

The IPP measures the velocity and flight time of particles in a fluidized bed. The data is used to calculate the geometrical length of the particles and stored in a ring buffer. This information is then used to determine the particle size distribution and velocity distributions. The IPP, which is capable of measuring particles ranging from 50 to 6000 µm in size and velocities of up to 50 m s^{-1}, is described in detail, including its technical specifications, in [18]. The internal air flush for dispersion was set to 15 L min^{-1}, and the external channel was flushed for cleaning every 20 seconds for two seconds with 2.5 L min^{-1}. The adjustment factor was set to one and no offset was defined. The ring buffer was set to 50000 particles which is the data set from which the current size distribution curve is calculated. The maximal loading was set to 50 %. At an average particle rate of approximately 1550 s^{-1}, depending on the degree of fluidization, the ring buffer is overwritten about every 30 seconds.

2.5. Off-line powder analysis

Particle size was measured by laser diffraction with a Mastersizer 2000 (Malvern Instruments GmbH, Herrenberg, Germany) with a dry dispersion unit at a dispersion pressure of 0.3 MPa. The moisture content was analyzed using Karl Fischer titration according to the method in [19]. A solvent consisting of 10 ml formamide and 20 ml methanol at a temperature of 50 °C and a titration time of 300 s was used for this purpose. Bulk density was measured according to EN ISO 60 using the bulk density tester SMG 53466 from Powtec Maschinen und Engineering GmbH (Remscheid, Germany). Measurements were performed in triplicate.

3. Results and Discussion

The results are presented in two parts. Firstly, the findings of the DoE are presented, and conclusions are drawn regarding the influence of the investigated factors (nozzle type, fluidization temperature and velocity, as well as binder spray rate) on the particle properties. Secondly, in-line monitoring systems for the product moisture content and the particle size distribution are evaluated. Regarding the product moisture content, capacitive moisture measurement and NIR measurement approaches were tested. The particle size distribution was measured in-line via the IPP, fitted to the Rosin-Rammler function and used for a PLS regression of the NIR spectra.

3.1 Spray through agglomeration with an integrated fluidized bed

Agglomeration in an integrated fluidized bed can be optimized by choosing the appropriate combination of process parameters. Therefore, the process conditions were varied in a wide range to give an overview of the spray through agglomeration process. In the following each investigated factor and its influences on the responses is described separately. Afterwards correlations between the responses are shown. Lastly, selected DoE results are illustrated.

Firstly, the nozzle type influences the size distribution obtained. For example, the results of the reference trials (80 °C, 0.8 m s^{-1}) under the same process conditions without

Preprints (www.preprints.org) | NOT PEER-REVIEWED | Posted: 12 June 2023 doi:10.20944/preprints202306.0844.v1

binder addition are shown in Figure 3. The pressure nozzle (diameter 0.3 mm) produced smaller agglomerates ($d_{50,3}$ = 43.82 µm) than the two-fluid nozzle ($d_{50,3}$ = 70.61 µm). The nozzle also affects the resulting bulk density, with the pressure nozzle producing higher bulk densities (535 to 609 kg m^{-3}) than the two-fluid nozzle (469 to 552 kg m^{-3}). The difference can be attributed to changes in the morphology and porosity of the primary particles, as well as the agglomerate structure. As stated in literature, without atomizing gas the porosity is lower, which can result in higher bulk densities. The pressure nozzle does not incorporate air into the droplets resulting in a decrease in bulk density. This higher density can result in faster sedimentation into the fluidized bed and potentially longer residence time. However, the smaller size and higher density of the particles produced by the pressure nozzle may also result in smaller agglomerates, probably due to collision probabilities, as sedimentation depends on size, shape and density of the particles [20]. The residence time in the system is determined by the powder level, and once this is constant, the powder is discharged.

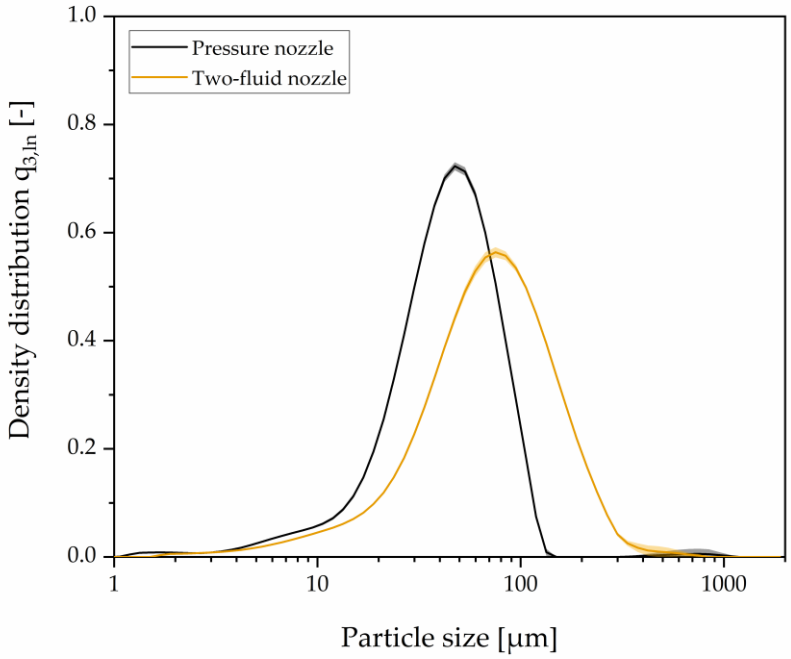

Figure 3. Particle size distributions of the reference (center) trial at the same process conditions with different nozzles used. The central experimental parameters were: Fluidized bed temperature: 80 °C, fluidization 0.8 m s^{-1} and no binding agent.

The second factor to consider is the influence of the fluidization temperature on the particle properties. Results show that the temperature alone had only minor effects on the particle properties. This is indicated by the highest correlations of this factor being found for humidity and water activity, with correlation coefficients of -0.34 and -0.39, respectively. Normally, an impact of temperature on the particle stickiness, as well as the corresponding changes in particle size, is expected due to the glass transition as thermal binding mechanism [8]. In the trial conducted with the two-phase nozzle at 0.6 m s^{-1} fluidization, 100 °C, and maximum binder dosage, a moisture level of 6.49 % was achieved. Literature shows that glass transition temperatures for SMP at this moisture level are around 26 °C. The glass transition temperature depends on material properties and the amount of plasticizer, e.g. water. In the viscous state above the onset glass transition temperature the surface viscosity is reduced and material stickiness enables agglomeration of particles. The sticky point is reached when the surface viscosity of the particles falls below a critical value, typically around 10 to 20°C above the onset glass transition temperature. [21] The fluidizing air was considerably above the sticky point temperature (55 K) indicating a high

Preprints (www.preprints.org) | NOT PEER-REVIEWED | Posted: 12 June 2023 doi:10.20944/preprints202306.0844.v1

particle cohesion probability. However, the measured particle size was 60.46 µm, which is similar for all DoE trials using the same nozzle. In addition to the cohesion probability, the collision probability influenced by the fluidization velocity is a factor controlling the agglomeration. Since the fluidization velocity showed only minor effects on particle properties, a better understanding of the cohesion and collision probabilities is necessary.

The amount of binding agent used had an impact on several factors, particularly moisture content (r = 0.67) and water activity. With increasing binder spray rate the moisture content of the particles increases, considering all samples in a common boxplot (Figure 4). The moisture content can be adjusted via the process parameters without the addition of binders. Median moisture contents of 4 % have been achieved, at which efficient agglomeration cannot be expected as the product is not sticky enough at the powder temperatures reached. The addition of binding agent enables the particles to enter the sticky region for agglomeration.

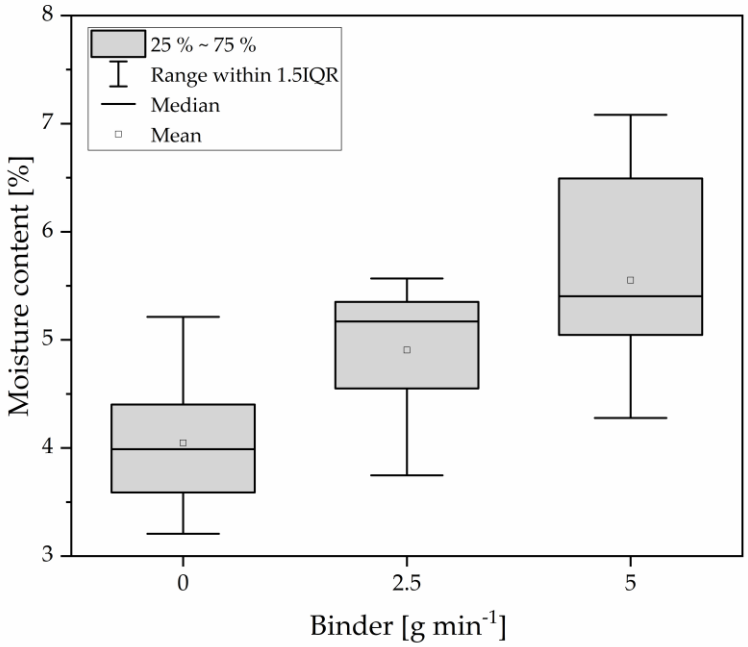

Figure 4. Boxplot of particle moisture as a function of binder addition. Evaluated are all experiments from the DoE, classified by spray rate.

The responses of the product were further analyzed (Table 1). As expected, a strong correlation was observed between moisture and water activity, which can be described by a product-specific sorption isotherm. Additionally, moisture was also moderately positive correlated moderately with particle size parameters, such as with the $D_{3,2}$ or the scale parameter. Conversely, the shape parameter correlated moderately negatively with moisture meaning that the distribution becomes broader with an increasing amount of binding agent. This is further supported by the increase of the span. The bulk density correlated both, offline and strongly in-line, with the CM sensor response.

Table 1. Correlation matrix of the investigated DoE responses.

	Water activity	$D_{3,2}$	x′ scale parameter	n shape parameter	CM offline	CM in-line
Moisture	0.920**	0.596*	0.592*	-0.650*	0,170	-0,403
Bulk density	-0,182	0,070	-0,289	0,216	0,520*	0.968**

*: moderate correlation, **: strong correlation

Preprints (www.preprints.org) | NOT PEER-REVIEWED | Posted: 12 June 2023 doi:10.20944/preprints202306.0844.v1

To understand the effect of the process on particle moisture and to determine the major influencing factors analysis of variance (ANOVA) techniques was used. To select a suited model description the center point was included to check for nonlinear correlations. The results showed that the moisture content curvature was not significant. Thus, the null hypothesis was rejected, and an unadjusted model was formed. The model mainly included effects of the binder spray rate (56.52 %), the fluidized bed temperature (14.22 %) and the interaction between the nozzle type and fluidization velocity (10.67 %). Non-significant interaction terms were also included to form a physically hierarchical model. The resulting model was significant ($p = 0.0002$) with an adjusted R^2 of 0.87. The diagnostic parameters were found to be acceptable, however, the residuals for the two-phase nozzle were observed to be larger but still within acceptable limits. The expected moisture is plotted as a function of the main influencing factors (Figure 5). The moisture content increases with higher binder spray rates and lower temperature providing a systematic understanding of how moisture can be influenced. This allows the moisture in the application to be changed if the sensors detect a deviation from the nominal value.

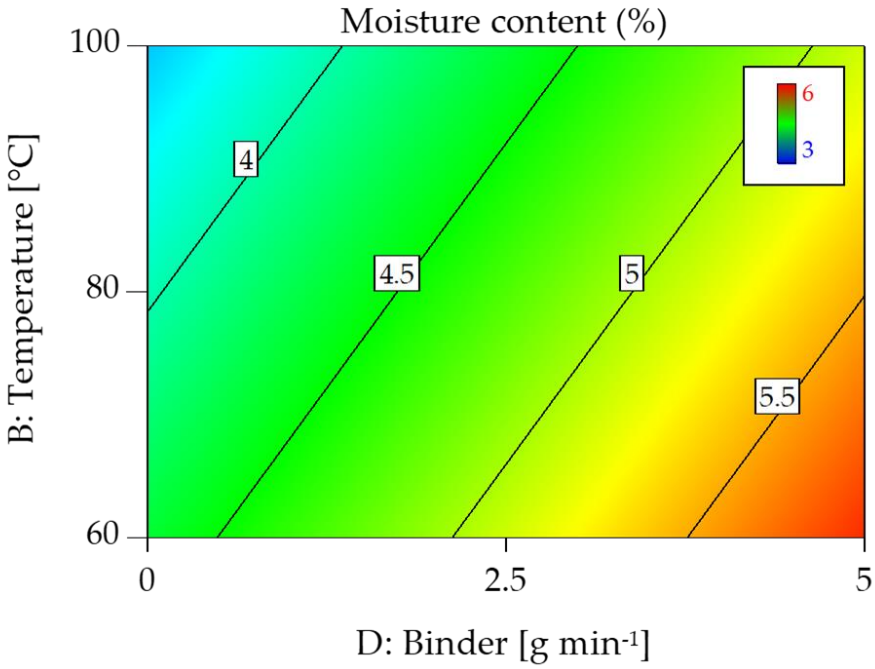

Figure 5. Contour plot of predicted moisture as a function of process conditions. Nozzle type is set to average and fluidization velocity to reference condition (0.8 m s^{-1}).

The variation of product moisture as shown in Figure 5, covering a range of 3.5 to 6 %, is relatively small. However, the product changes within this range from a full cohesionless material to a highly sticky powder that agglomerates easily. Controlling this critical product change is the challenge to be solved by the use of the implemented in-line measurement and control system. The multi-stage design of the process has the benefit of a process integration, but also the particular drawback that less control parameters can be adjusted to ensure a robust and optimal performance.

3.2 Capacitive sensor responses

The objective was to determine if the CM sensor can accurately and reliably measure the moisture content. Firstly, regression was performed for the offline sensor responses, but it was found that the coefficients of determination were low. Specifically, the R^2 value was 0.33 for the pressure nozzle and 0.28 for the two-phase nozzle. Combining the data sets for a combined regression did not improve the model (data not shown). Kupfer [21] emphasized the bulk density as one of the most important influences on indirect water determination. When the offline sensor response is correlated to the bulk densities of the powder, a R^2 of 0.76 is achieved for the pressure nozzle and of 0.91 for the two-phase

Preprints (www.preprints.org) | NOT PEER-REVIEWED | Posted: 12 June 2023 doi:10.20944/preprints202306.0844.v1

model (Figure 6). Consequently, the effect of the bulk density on the sensor response is more pronounced than the effect of the moisture content.

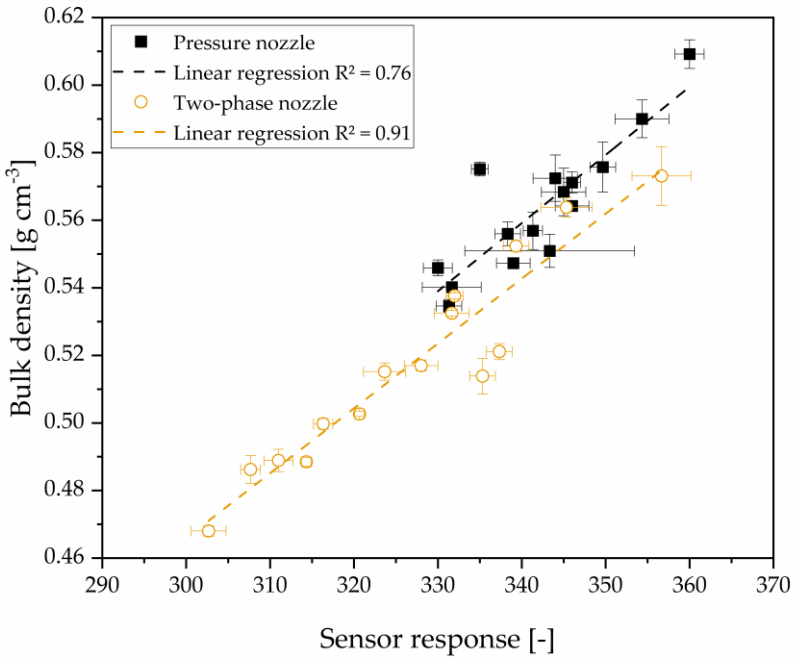

Figure 6. Linear regression of the offline measurement data from the capacitive moisture sensor to the bulk density.

The in-line sensor response showed no correlation with the water content, indicated by an R^2 of 0.14 for the pressure nozzle trials and 0.01 for the two-phase nozzle trials. (data not shown) However, it was found to be positively correlated with the pressure drop and filling level of the fluidized material. The correlation was affected by the interval at which pneumatic hammers release material from the spray dryer wall occurring every 60 seconds. This relationship is illustrated as an example (Figure 7). By varying the frequency of the pneumatic hammers, frequency dependency was demonstrated (data not shown).

Similar effects with capacitive sensors have been reported in literature, where it was necessary to calibrate at high moisture levels (up to 70 %), assuming consistent material thickness and density [23]. Due to variances and a lack of mathematical patterns, corrections for material thickness and density were unsuccessful. Li et al. [24] summarized constraints for the moisture measurement of corn related to product properties, i.e. flow state or pore distribution. In these circumstances, NIR sensors have been favored. Recent research indicates that in fluidized beds, a dependence on process and product conditions is more prevalent for CM sensors compared to NIR sensors [25]. One possible way to gain a better understanding of the underlying mechanisms is using pressure fluctuation analysis, as demonstrated by J. C. Schouten and colleagues. This method can provide valuable insights that can help refine and optimize the multi-sensor approach for early detection of system changes [26].

Preprints (www.preprints.org) | NOT PEER-REVIEWED | Posted: 12 June 2023 doi:10.20944/preprints202306.0844.v1

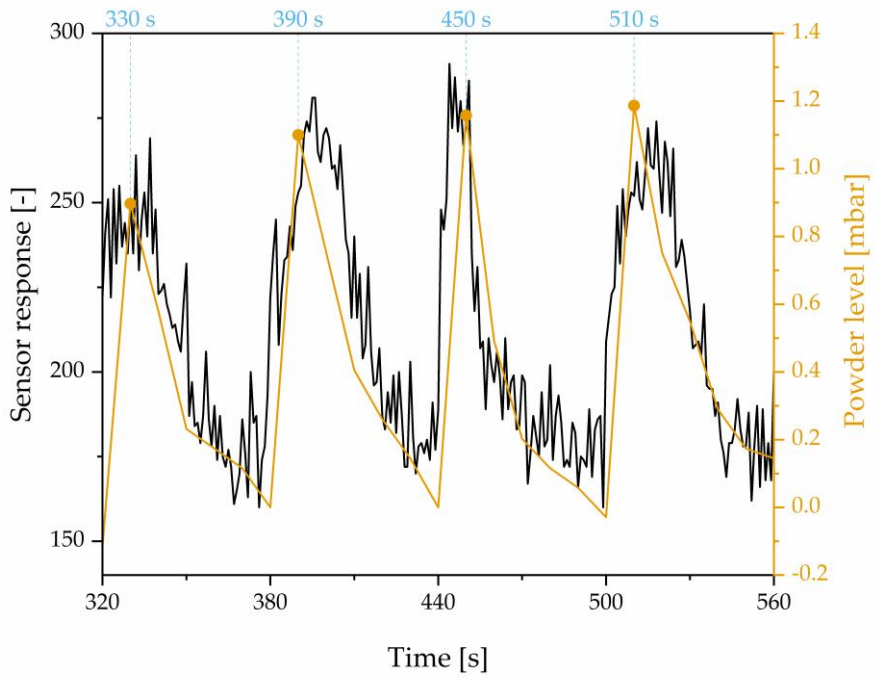

Figure 7. Sensor response over time of the CM Sensor. The 60 seconds intervals of the pneumatic hammers are reflected in the sensor signal.

3.3 Calibration of near-infrared spectra to the moisture content

In this chapter, the building of the NIR model via PLS regression to predict the moisture content in the integrated fluidized bed in-line is presented. Different selection of spectral data was tested as the NIR spectra varied with the type of nozzle used for atomizing the feed. Despite these differences, a joint model was established to predict the properties of the powder samples independent of the nozzle type used. However, if necessary, better correlations with fewer resulting factors from the PLS can be achieved by using separate models for each nozzle type. The last minute before taking the sample was averaged for further evaluation.

To correct the spectral data for noise, baseline shifts or scaling differences various pre-processing techniques were tested systematically. This can enhance the model robustness or reduce the number of factors needed. The optimum number of factors for each pre-processing was evaluated using multivariate statistical parameters (Table 2). Afterwards, a pre-processing is suggested according to the lowest number of factors, highest R^2 and lowest errors of the model as indicated in the table. The most suitable method chosen was the standard normal variate (SNV) with eight factors.

Table 2. Comparison of different pre-processing techniques and the number of factors included in the PLS model.

Pre-processing	No. of factors	R^2 (C)	R^2 (V)	RMSEC	RMSEP	SEC	SEP	Bias
None	2	0.30	0.31	1.17	1.16	1.18	1.19	2e-16
Smoothing	2	0.30	0.30	1.17	1.16	1.18	1.19	-4e-16
Detrending	3	0.75	0.69	0.70	0.78	0.70	0.80	5e-16
SNV	8	0.94	0.83	0.33	0.58	0.33	0.59	-3e-15
1st derivative	5	0.81	0.71	0.62	0.75	0.62	0.76	7e-16
2nd derivative	4	0.75	0.65	0.70	0.83	0.70	0.85	9e-16
MSC	8	0.95	0.81	0.33	0.61	0.33	0.62	-3e-14

Preprints (www.preprints.org) | NOT PEER-REVIEWED | Posted: 12 June 2023 doi:10.20944/preprints202306.0844.v1

The scores indicate the coordinates of the objects in the factor space. A selection of scores for two factors classified in four groups of different moisture contents (Figure 8a) shows a lower moisture content for lower factors 3 and 6 and vice versa. However, using only two factors the samples could not be separated clearly in the factor space according to their moisture content. This emphasizes the need for more factors in the PLS model due to various influences in-line in the spray dryer on the spectral data. When considering the loadings for these two factors (Figure 8b), the wavelength region between 1400 and 1500 nm (blue) shows a positive impact on the moisture content. This region correlates with the second overtone of the OH, CH and CH_2 group. The wavelength region between 1350 and 1400 nm (green), where the second overtone of the CH_2 and CH_3 group is located, has an opposed effect for factor 3 and 6.

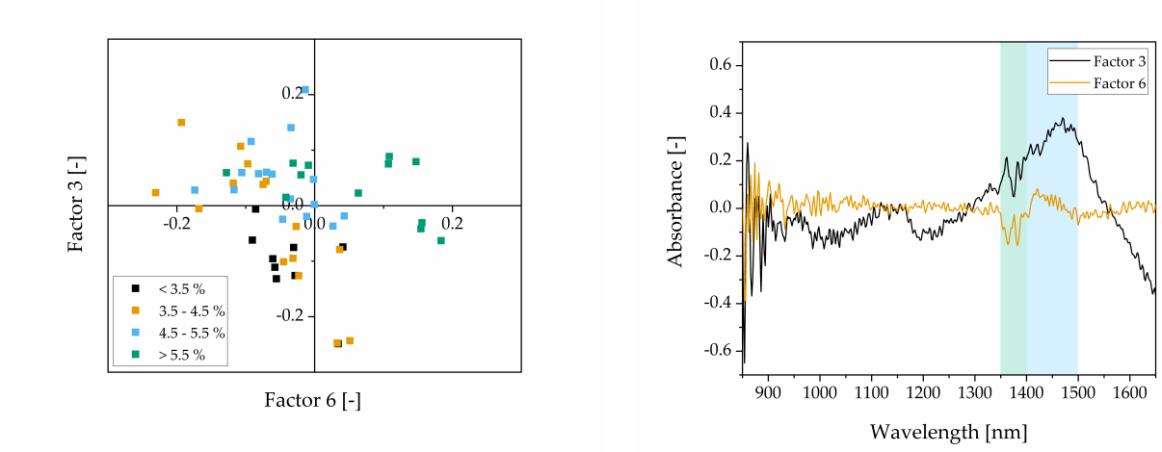

(**a**) (**b**)

Figure 8. Selection of (**a**) the scores and (**b**) the loadings of factor 3 and 6 for prediction of the moisture content via PLS regression.

The predicted moisture is plotted over the measured moisture based on titration (Figure 9). The R^2 was 0.94 and the root mean square error (RMSE) was 0.33 %. The linear regression with confidence and prediction interval is illustrated for the calibration data set.

Preprints (www.preprints.org) | NOT PEER-REVIEWED | Posted: 12 June 2023 doi:10.20944/preprints202306.0844.v1

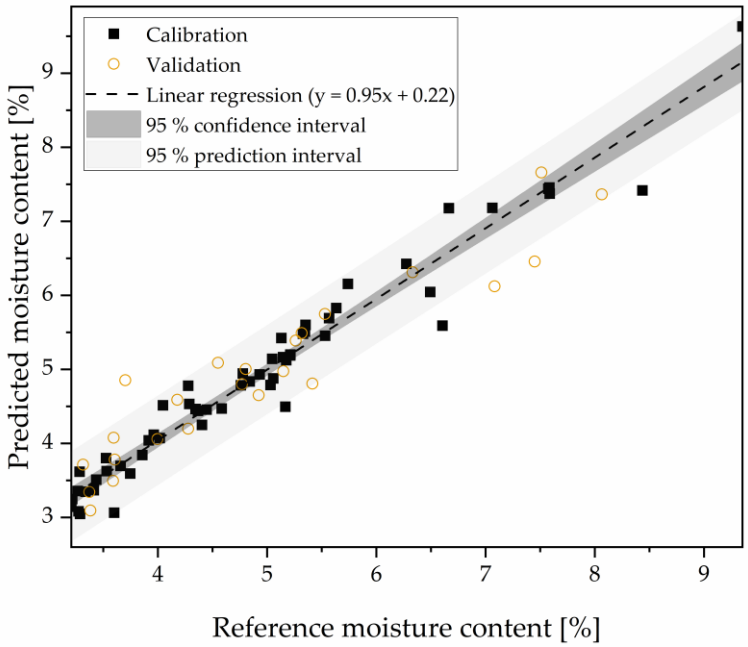

Figure 9. Measured water content compared to predicted water content for calibration and validation data set (n = 80) with linear regression.

The model predicts a moisture content of the agglomerates between 3 and 9.5 %. From pre-trials, it has been shown that low moisture contents (< 3 %) can only be achieved without the addition of binders and with extended post-drying, while high moisture contents above about 10 % led to blockage of the fluidized bed. To conclude, the final model includes all relevant process regions for the manufacture of SMP in this spray drying set-up.

In the literature, the pre-processings and number of factors vary for comparable PLS models. SNV pre-processing was used in predictions from offline and online built models [27-28]. This standardization corrects for scattering effects due to differences in the physical properties of the samples, mainly the particle size, and is commonly used for particulate systems. The number of factors depended on the complexity of the samples. While only a few factors were needed for models measured offline [27] or with similar material [29], more than 10 factors were considered for dairy samples with different fat content, animal type, producer, etc [28]. Maltesen et al. [27] also found, that the morphology of the samples had a significant impact on the predictive ability of the models and recommended using smooth and spherical particles. This explains the number of factors used for the PLS model in this study as different nozzle types produce different particle morphology. Further, different process conditions can lead to a change in the in-line NIR signal.

3.4 Calibration of near-infrared spectra to particle size distribution using Rosin-Rammler fit

Analogous to the moisture content, the aim was to estimate the particle size within the fluidized bed using the scattered light data from the NIR spectra. Instead of basing the model on the particle sizes measured externally in the laboratory the model was based on the cumulative distribution curves obtained in-line using the IPP probe. The advantage of this approach is that the process can be continuously reflected, and a higher number of samples can be analyzed over time with varying process parameters. Further, the acquisition of the particle size is less complex compared to a subsequent laboratory analysis as no samples need to be taken. However, it should be noted that the in-line measurement

Preprints (www.preprints.org) | NOT PEER-REVIEWED | Posted: 12 June 2023 doi:10.20944/preprints202306.0844.v1

method also deviates from the laboratory results. This deviation is attributed to the different measurement principles as well as the limitations in the lower particle size. The measuring position within the fluidized bed may also lead to a non-representative sampling of the particles. The use of a single, non-invasive probe to simultaneously obtain information about both, the moisture and particle size distribution of the sample, holds potential by indicating the success of agglomeration in real time.

After fitting the IPP data to the cumulative distribution function (CDF) of the Rosin-Rammler distribution (Equation 1, [30]), the scale and shape parameters were extracted as output variables for the models. A separate model was developed for each parameter

$$Q_3(x) = 1 - exp\left(-\left(\frac{x}{x'}\right)^n\right) \quad (1)$$

with x' as scale and n as shape parameter.

The selected number of factors and the corresponding statistical parameters for the different pre-processings are listed in Table 3. The algorithm suggests no pre-processing and 15 factors. Alternatively, the second derivative with 17 factors could be considered, but was excluded as the model did not show an improvement in the prediction.

Table 3. Comparison of different pre-processing techniques and the number of factors included in the PLS model.

Pre-processing	No. of factors	R^2 (C)	R^2 (V)	RMSEC	RMSEP	SEC	SEP	Bias
None	15	0.96	0.94	8.18	9.63	8.20	9.68	9e-13
Smoothing	13	0.92	0.92	10.94	10.69	10.96	10.76	4e-13
Detrending	12	0.94	0.93	10.09	10.09	9.86	10.14	1e-13
SNV	3	0.33	0.32	31.79	31.79	34.38	31.97	3e-15
1st derivative	14	0.94	0.93	9.62	9.62	9.54	9.68	3e-14
2nd derivative	17	0.94	0.84	9.12	9.12	7.82	9.17	4e-14
MSC	12	0.90	0.90	12.40	12.40	11.76	12.47	-9e-13

The scores and loadings for factor 8 and 9 of the PLS model are evaluated as an example. For those two factors the scale parameter is lowest with negative score values and increases with increasing score values, which is indicated via 4 differently colored groups (Figure 10a). However, no explicit separation is possible by only two factors. Regarding the loadings, a clear peak over both factors was not noticeable and opposing trends per wavelength can be seen (Figure 10b).

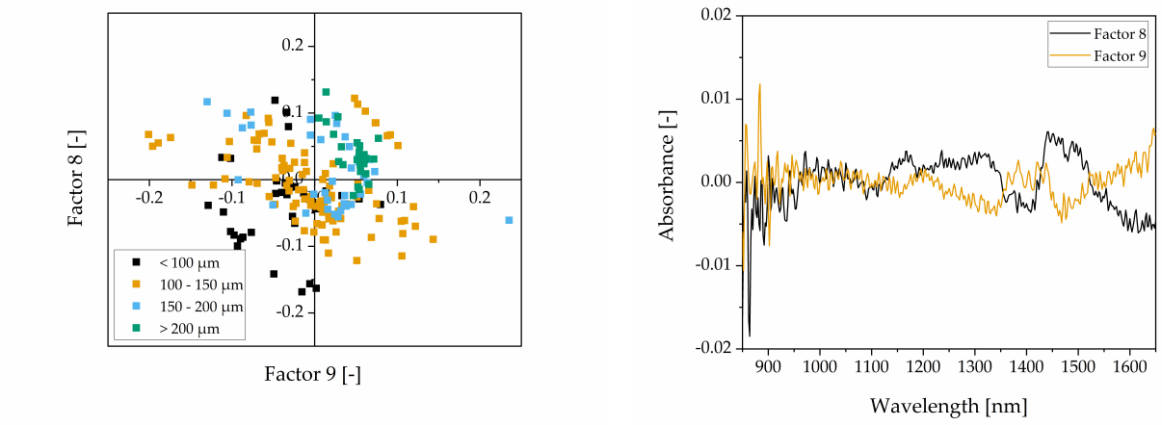

(**a**) (**b**)

Figure 10. Selection of (**a**) the scores and (**b**) the loadings of factor 8 and 9 for prediction of the scale parameter via PLS regression.

Preprints (www.preprints.org) | NOT PEER-REVIEWED | Posted: 12 June 2023 doi:10.20944/preprints202306.0844.v1

The resulting prediction from the PLS with 15 factors and no pre-processing is compared with the measured values (Figure 11). The scale parameter x' in µm is shown and fitted well between 60 and 210 µm. The precision of the fit is represented by R^2 values with 0.96 and a RMSE of 8.18. The maximum deviation of the validation set predictions was 24 µm or 16 % of the data spread of 150 µm. This indicates that the model is able to make reliable predictions.

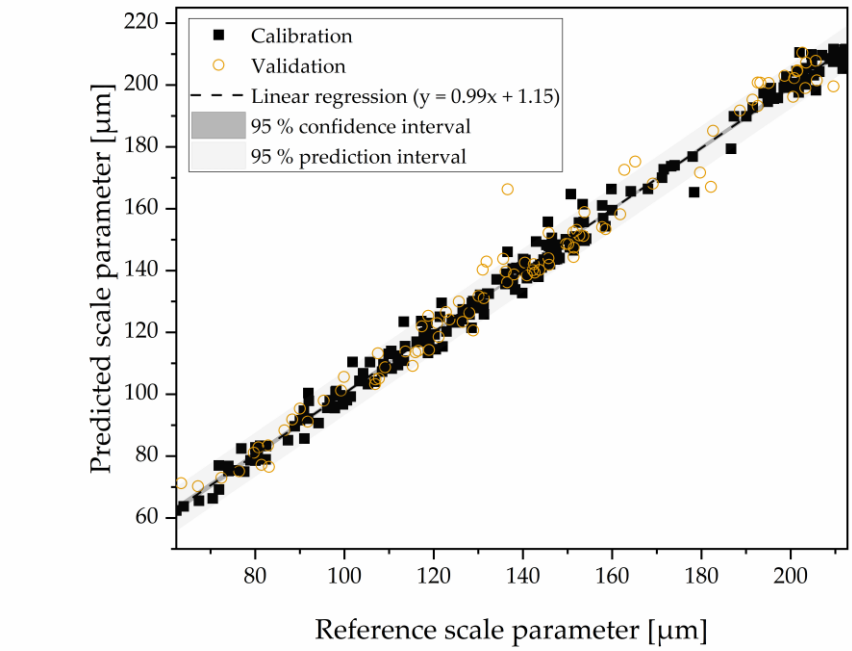

Figure 11. Measured compared to predicted scale parameter x' for calibration and validation data set (n = 294) with linear regression.

The same procedure was followed for the shape parameters n in a range between 1.8 and 3.1. Different pre-processings were compared according to multivariate statistics and the raw spectra with 17 factors, a R^2 of 0.92 and a RMSE of 0.06 were suggested by the algorithm (Table 4). The maximum deviation of the validation set predictions was 0.34 or 20 % of the data spread of 1.7 µm. The particle size distribution and the resulting fluidization behavior can lead to a changed scattering effect, which is a change in amount and direction of the reflected light. This change results mainly in baseline shifting and noise [31]. As the principle of pre-processing is to reduce the noise and the baseline shift from the spectral data, the information about particle size is only present in the models without any pre-processing or those without baseline correction.

Table 4. Comparison of different pre-processing techniques and the number of factors included in the PLS model.

Pre-processing	No. of factors	R^2 (C)	R^2 (V)	RMSEC	RMSEP	SEC	SEP	Bias
None	17	0.92	0.89	0.06	0.07	0.06	0.07	-6e-15
Smoothing	4	0.29	0.28	0.18	0.19	0.18	0.19	6e-16
Detrending	17	0.93	0.90	0.05	0.07	0.05	0.07	-8e-16
SNV	2	0.22	0.24	0.19	0.19	0.19	0.20	-2e-16
1st derivative	9	0.82	0.79	0.09	0.10	0.09	0.10	-8e-16
2nd derivative	5	0.64	0.68	0.13	0.13	0.13	0.13	-1e-16
MSC	2	0.32	0.27	0.17	0.19	0.18	0.19	6e-16

Preprints (www.preprints.org) | NOT PEER-REVIEWED | Posted: 12 June 2023 doi:10.20944/preprints202306.0844.v1

The scores of factors 15 and 16 are illustrated as an example grouped by shape parameter via different colors (Figure 12a). The smaller shape parameters < 2 are located in the third quadrant with negative score values for both factors, while the bigger shape parameters > 3 are present in the first quadrant with positive score values. However, no separation in the factor space is possible via two factors. The loadings show no clear peaks and high noise for the lower wavelengths (Figure 12b).

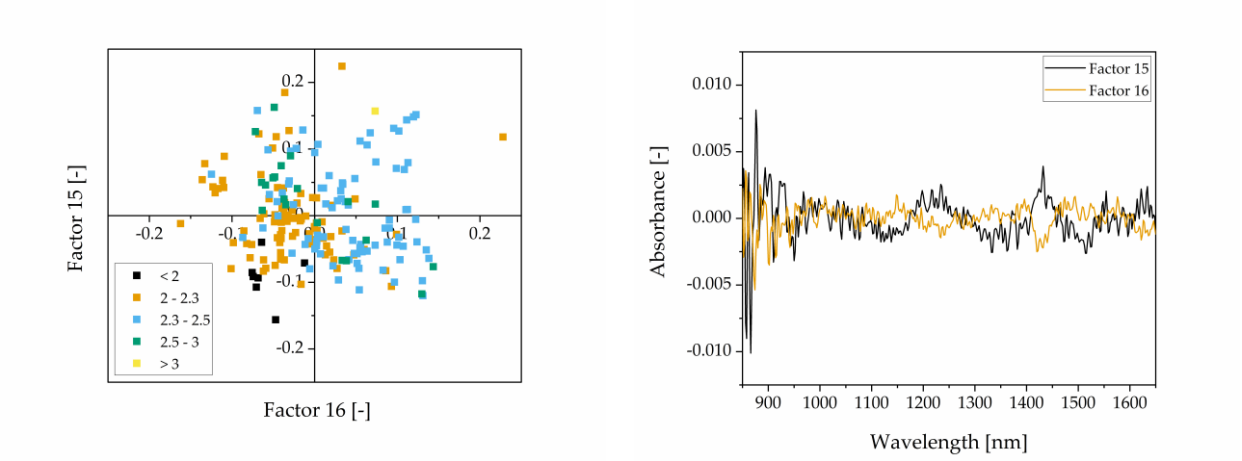

(**a**) (**b**)

Figure 12. Selection of (**a**) the scores and (**b**) the loadings of factor 15 and 16 for prediction of the shape parameter via PLS regression.

The predicted shape parameter is plotted over the reference shape parameter for the calibration and the validation data set with a linear regression and corresponding 95 % confidence and prediction intervals (Figure 13). The evaluated range represents similar particle size distributions and shows a lower data density with shape parameters above 2.7. For a robust prediction the extension of the model is necessary.

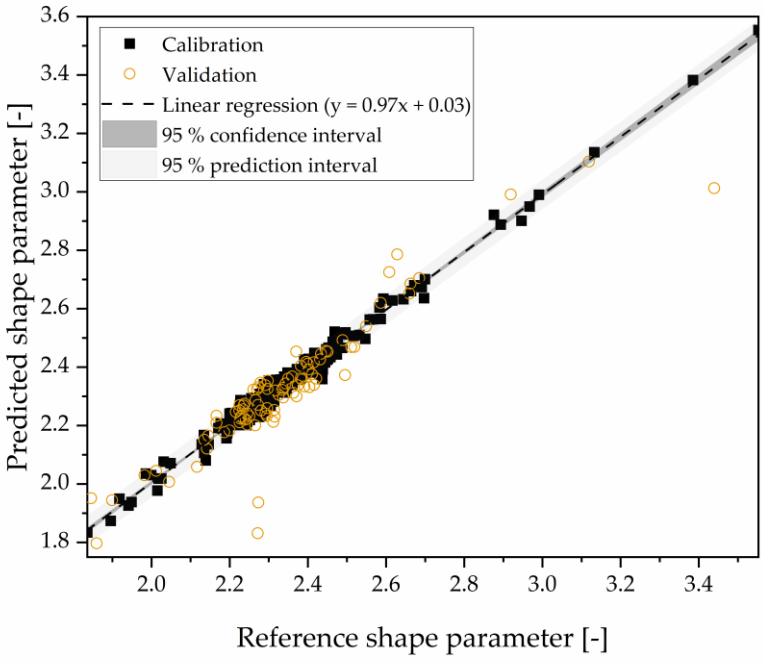

Figure 13. Measured compared to predicted shape parameter n or calibration and validation data set (n = 294) with linear regression.

 doi:10.20944/preprints202306.0844.v1

The model building methodology employed in this study was successful, as it allowed for the fitting of the particle size distribution, not only through a single parameter, such as the median particle diameter [32], but also by approximating the entire distribution curve using a Rosin-Rammler fit. The model is able to predict the particle size distribution in application from the raw spectra with 15 and 17 factors, as demonstrated by the results in Figures 11 and 13. A high number of factors needed was expected, because physical information about particle size distribution and morphology can be found in baseline offset and noise across the entire spectrum [27, 31]. Contrary, Higgins et al [33] were able to predict the d_{90} in an online milling process with one factor, where their samples had a broad size range, but did not differ in chemical composition. This emphasizes the influence of the particle morphology on the spectrum [27]. In literature different effects of the particle size distribution on the spectral data are observed, but additional investigation of the underlying principle is required, especially regarding the influence of the particle morphology. Further, an effect from the movement of the particles in the fluidized bed on the NIR signal cannot be excluded.

4. Conclusions

This study analyzed the spray drying process with forced agglomeration in an integrated fluidized bed in terms of nozzle type and key influencing factors such as binder rate, fluidization velocity and temperature. These factors were varied to examine their effect on the particle moisture and size. The NIR sensor calibration allowed to determine the moisture content with an RMSE of 0.33 %, although the CM sensor calibration was insufficient. It is currently believed that the primary effect seen in CM measurements is due to changes in cohesion, resulting in changes in fluidization patterns. Further investigation and validation of these assumptions is necessary to ensure the accuracy and effectiveness of this approach. Surprisingly, the non-invasive NIR sensor enabled the prediction of particle size distribution with scale and shape parameters of the Rosin-Rammler fit. The use of a multi-sensor approach as a tool for very early detection of system changes is a promising concept with enormous potential for improving quality control by checking for unexpected deviations from the sensors. Regarding the process integration, this approach is particularly useful in knife-edge process situations where even small changes in the system may have a significant impact on product quality or process stability. However, to fully realize the potential of this method, it will be necessary to conduct more detailed analyses of a broader range of systems.

Author Contributions: Conceptualization, J.F., T.R. and R.K.; methodology, J.F and T.R.; software J.F.; validation, L.G.; formal analysis, J.F., T.R. and L.G.; investigation, J.F., T.R. and L.G.; resources, R.K.; data curation, J.F and T.R.; writing—original draft preparation, J.F., T.R. and L.G.; writing—review and editing, J.F., T.R. and R.K..; visualization, J.F and T.R.; supervision, J.F., T.R. and R.K.; project administration, J.F and T.R.; funding acquisition, R.K. All authors have read and agreed to the published version of the manuscript.

Funding: This IGF project 20952 N of the FEI is/was supported within the program for promoting the Industrial Collective Research (IGF) of the German Ministry of Economics and Climate Action (BMWK), based on resolution of the German Parliament.

Conflicts of Interest: The authors declare no conflict of interest.

References

1. *Encyclopedia of food and health;* Caballero, B.; Finglas, P.M.; Toldrá, F., Eds., 3rd ed.; Elsevier Acad. Press: Amsterdam, 2016, ISBN 9780123849472.
2. Kessler, H.-G. *Lebensmittel- und Bioverfahrenstechnik*: *Molkereitechnologie; mit 109 Tabellen*, 4., überbearb. und erw. Aufl., 1. Nachdr; Verl. A. Kessler: München, 2006, ISBN 3-9802378-4-2.
3. *Modern Drying Technology*: *Volume 3: Product Quality and Formulation;* Tsotsas, E.; Mujumdar, A.S., Eds.; Wiley-VCH: Weinheim, 2007, ISBN 978-3-527-31558-1.
4. Turchiuli, C.; Gianfrancesco, A.; Palzer, S.; Dumoulin, E. Evolution of particle properties during spray drying in relation with stickiness and agglomeration control. *Powder Technology* **2011**, *208*, 433–440, doi:10.1016/j.powtec.2010.08.040.

5. Palzer, S. Agglomeration of pharmaceutical, detergent, chemical and food powders — Similarities and differences of materials and processes. *Powder Technology* **2011**, *206*, 2–17, doi:10.1016/j.powtec.2010.05.006.
6. Williams, A.M. Instant milk powder production: determining the extent of agglomeration: A thesis presented in partial fulfilment of the requirements for the degree of Doctor of Philosophy. Dissertation; Massey University, Palmerston North, New Zealand, 2007.
7. Písecký, J. *Handbook of milk powder manufacture*, 2. edition, 1. oplag; GEA Niro: Soeborg, 2012, ISBN 87-87036-74-6.
8. Bück, A.; Tsotsas, E. Agglomeration. In *Encyclopedia of Food and Health*; Caballero, B., Toldrá, F., Finglas, P.M., Eds.; Elsevier Science: Burlington, United Kingdom, 2015; pp 73–81, ISBN 9780123849533.
9. Schwartzbach, C.; Masters, K. Perfomance of spray dryer with integrated filter and fluid bed. *Drying Technology* **2001**, *19*, 1909–1923, doi:10.1081/DRT-100107279.
10. Jones, D.M. Factors to consider in fluid-bed processing. *Pharmaceutical technology* **1985**, *9*, 50–55.
11. Demers, A.-M.; Gosselin, R.; Simard, J.-S.; Abatzoglou, N. In-line near infrared spectroscopy monitoring of pharmaceutical powder moisture in a fluidised bed dryer: An efficient methodology for chemometric model development. *Can. J. Chem. Eng.* **2012**, *90*, 299–303, doi:10.1002/cjce.20691
12. Fischer, C.; Jaskulski, M.; Tsotsas, E. Inline method of droplet and particle size distribution analysis in dilute disperse systems. *Advanced Powder Technology* **2017**, *28*, 2820–2829, doi:10.1016/j.apt.2017.08.009.
13. Burggraeve, A.; Silva, A.F.T.; van den Kerkhof, T.; Hellings, M.; Vervaet, C.; Remon, J.P.; Vander Heyden, Y.; Beer, T. de. Development of a fluid bed granulation process control strategy based on real-time process and product measurements. *Talanta* **2012**, *100*, 293–302, doi:10.1016/j.talanta.2012.07.054.
14. Frake, P.; Greenhalgh, D.; Grierson, S.M.; Hempenstall, J.M.; Rudd, D.R. Process control and end-point determination of a fluid bed granulation by application of near infra-red spectroscopy. *Int. J. Pharm.* **1997**, *151*, 75–80, doi:10.1016/S0378-5173(97)04894-1.
15. Hede, P.D.; Bach, P.; Jensen, A.D. Top-spray fluid bed coating: Scale-up in terms of relative droplet size and drying force. *Powder Technology* **2008**, *184*, 318–332, doi:10.1016/j.powtec.2007.09.009.
16. Fröhlich, J.A.; Ruprecht, N.A.; Hinrichs, J.; Kohlus, R. Nozzle zone agglomeration in spray dryers: Effect of powder addition on particle coalescence. *Powder Technology* **2020**, *374*, 223–232, doi:10.1016/j.powtec.2020.07.009.
17. Qurthobi, A.; Iskandar, R.F.; Krisnatal, A.; Weldzikarvina. Design of capacitive sensor for water level measurement. *J. Phys.: Conf. Ser.* **2016**, *776*, 12118, doi:10.1088/1742-6596/776/1/012118.
18. Petrak, D.; Dietrich, S.; Eckardt, G.; Köhler, M. In-line particle sizing for real-time process control by fibre-optical spatial filtering technique (SFT). *Advanced Powder Technology* **2011**, *22*, 203–208, doi:10.1016/j.apt.2010.11.002.
19. Isengard, H.-D.; Haschka, E.; Merkh, G. Development of a method for water determination in lactose. *Food Chem.* **2012**, *132*, 1660–1663, doi:10.1016/j.foodchem.2011.04.100.
20. Fröhlich, J.A.; Raiber, T.V.; Hinrichs, J.; Kohlus, R. Nozzle zone agglomeration in spray dryers: Influence of total solid content on agglomerate properties. *Powder Technology* **2021**, *390*, 292–302, doi:10.1016/j.powtec.2021.05.094.
21. Silalai, N.; Roos, Y.H. Roles of water and solids composition in the control of glass transition and stickiness of milk powders. *J. Food Sci.* **2010**, *75*, E285-96, doi:10.1111/j.1750-3841.2010.01652
22. Kupfer, K. *Materialfeuchtemessung*: *Grundlagen, Messverfahren, Applikationen, Normen ; mit 19 Tabellen und 386 Literaturstellen;* Expert-Verl.: Renningen-Malmsheim, 1997, ISBN 3816913598.
23. Kormann, G. Untersuchungen zur Integration kontinuierlich arbeitender Feuchtemeßsysteme in ausgewählte Futtererntemaschinen. Dissertation; Technische Universität München, Freising-Weihenstephan, 2001.
24. Li, C.; Zhang, X.; Meng, M.; Li, B.; Li, C. Capacitive Online Corn Moisture Content Sensor Considering Porosity Distributions: Modeling, Design, and Experiments. *Applied Sciences* **2021**, *11*, 7655, doi:10.3390/app11167655.
25. Frank, J.; Schlitter, M.; Hinrichs, J.; Kohlus, R. Fluidized bed drying of dairy gel granules supported by in-line monitoring of the water content. *Drying Technology* **2023**, 1–11, doi:10.1080/07373937.2023.2216774.
26. Schouten, J.C.; Stappen, M. Van der; Bleek, C.M. Van den. Scale-up of chaotic fluidized bed hydrodynamics. *Chemical Engineering Science* **1996**, *51*, 1991–2000, doi:10.1016/0009-2509(96)00056-5.
27. Maltesen, M.J.; van de Weert, M.; Grohganz, H. Design of experiments-based monitoring of critical quality attributes for the spray-drying process of insulin by NIR spectroscopy. *AAPS PharmSciTech* **2012**, *13*, 747–755, doi:10.1208/s12249-012-9796-1.
28. Wang, C.; Reis, M.G.; Waterhouse, G.I.; Hemar, Y.; Reis, M.M. Prediction of dairy powder functionality attributes using diffuse reflectance in the visible and near infrared (Vis-NIR) region. *International Dairy Journal* **2021**, *117*, 104981, doi:10.1016/j.idairyj.2021.104981.
29. Aoki, H.; Hattori, Y.; Sasaki, T.; Otsuka, M. Comparative study on the real-time monitoring of a fluid bed drying process of extruded granules using near-infrared spectroscopy and audible acoustic emission. *Int. J. Pharm.* **2022**, *619*, 121689, doi:10.1016/j.ijpharm.2022.121689.
30. Stieß, M. *Mechanische Verfahrenstechnik - Partikeltechnologie 1*, 3., vollst. neu bearb. Aufl.; Springer Berlin Heidelberg: Berlin, Heidelberg, 2009, ISBN 978-3-540-32551-2.
31. Kessler, W. *Multivariate Datenanalyse*: *für die Pharma-, Bio- und Prozessanalytik;* Wiley-Blackwell: Weinheim, 2007, ISBN 978-3-527-31262-7.
32. Jukka Rantanen; Jouko Yliruusi. Determination of Particle Size in a Fluidized Bed Granulator With a Near Infrared Set-up. *Pharmacy and Pharmacology Communications* **1998**, *4*, 73–75, doi:10.1111/j.2042-7158.1998.tb00509.x.

 doi:10.20944/preprints202306.0844.v1

33. Higgins, J.P.; Arrivo, S.M.; Thurau, G.; Green, R.L.; Bowen, W.; Lange, A.; Templeton, A.C.; Thomas, D.L.; Reed, R.A. Spectroscopic approach for on-line monitoring of particle size during the processing of pharmaceutical nanoparticles. Anal. Chem. 2003, 75, 1777–1785, doi:10.1021/ac0207980.